ELSEVIER

Comparison of predicted and experimental Nusselt number for a film-cooled rotating blade

Vijay K. Garg
AYT Corporation, c/o NASA-Lewis Research Center, Cleveland, Ohio, USA

Reza S. Abhari
Department of Aerospace Engineering, Applied Mechanics and Aviation, The Ohio State University, Columbus, Ohio, USA

The predictions from a three-dimensional (3-D) Navier–Stokes code have been compared to the Nusselt number data obtained on a film-cooled, rotating turbine blade. The blade chosen is the ACE rotor with five rows containing 93 film-cooling holes covering the entire span. This is the only film-cooled rotating blade on which experimental heat transfer data are available for the present comparison. Over 2.25 million grid points are used to compute the flow over the blade. Usually, in a film cooling computation on a stationary blade, the computational domain is just one spanwise pitch of the film-cooling holes, with periodic boundary conditions in the span direction. However, for a rotating blade, the computational domain consists of the entire blade span from hub to tip, as well as the tip clearance region. As far as the authors know, the present work is the first comparison of the prediction of surface heat transfer using a 3-D Navier–Stokes code with film injection and the measured heat flux on a fully film-cooled rotating transonic turbine blade. A reasonably good comparison with the measured data is obtained on the suction surface, particularly near the hub section. On the pressure surface, however, the comparison between the data and the prediction is poor. A potential reason for the discrepancy on the pressure surface could be the presence of unsteady effects caused by stator–rotor interaction in the experiments, which are not modeled in the present numerical computations. © 1997 by Elsevier Science Inc.

Keywords: film cooling; three-dimensional Navier–Stokes analysis; rotating blade

Introduction

To extend component life, using film cooling in the design of turbine airfoils is widespread. To minimize the use of coolant flow, designers must have an accurate prediction of the component heat load and film-cooling effectiveness. The harsh operational environment as well as the high rates of rotational speed have combined to slow the progress in the understanding of the blade surface heat load in the presence of film cooling. Many studies on film cooling have been confined to simple geometries, for example, two-dimensional (2-D) flat and curved plates in steady, incompressible flow. An excellent survey of the work up to 1971 has been provided by Goldstein (1971). Several subsequent studies in this field have been summarized by Garg and Gaugler (1993, 1994, 1996), and some relevant ones are discussed here.

Three detailed experimental measurements of film cooling on rotating turbine blades are available in the literature. These investigations were presented by Dring et al. (1980), Abhari (1991), and Takeishi et al. (1991). All three studies concluded that film cooling on the suction surface provides good surface protection; whereas, on the pressure surface the results are mixed. The measurement database of Abhari (1991), being the only experimental measurement of surface heat transfer for a film-cooled rotating transonic turbine blade, provides the experimental results for the present numerical study. Abhari and Epstein (1994) also showed that the unsteady rotor–stator interaction results in the pulsation of the film cooling out of the holes. This coolant pulsation was later shown by Abhari (1996) to result in a considerable reduction on the pressure surface film effectiveness, while the suction surface was relatively unaffected.

In the past few years, advances in numerical techniques have resulted in the development of a number of different approaches specifically related to the study of film cooling. Many different approaches to the prediction of film cooling performance have been developed. By far the most prevalent approach has been to model or correlate the penetration, spreading, and entrainment of the main flow by the coolant jets from the discrete

Address reprint requests to Dr. V. K. Garg, c/o NASA-Lewis Research Center, AYT Corporation, Mail Stop 5-11, Cleveland, OH 44135-3191, USA.

Received 6 November 1996; accepted 5 March 1997

Int. J. Heat and Fluid Flow 18: 452–460, 1997
© 1997 by Elsevier Science Inc.
655 Avenue of the Americas, New York, NY 10010

0142-727X/97/$17.00
PII S0142-727X(97)00031-3

holes. These interaction models have been incorporated into boundary-layer codes (Crawford et al. 1980; Schonung and Rodi 1987; Tafti and Yavuzkurt 1990) or into 2-D Navier–Stokes CFD code (Abhari 1996). In another approach, Garg and Gaugler (1993, 1994, 1996, 1997a, 1997b) used a three-dimensional (3-D) CFD code with surface injection to model the film-cooling performance around the C3X vane and the VKI and ACE rotor cascades. In this approach, similar to the present technique, the film holes are modeled by adding, as a boundary condition, the appropriate amount of mass, momentum, and energy flux distribution at the discrete location of the film holes. They compared the predictions to the experimental measurements on these cascades and found a fairly good agreement. The computational results clearly illustrated the three-dimensionality of the flow in the near hole region. Choi (1993) also used a 3-D CFD code to predict the flow and the surface heat transfer around a section of the ACE turbine blade. The computational grid was extended into the film holes to model the elliptic nature of the flow at the film hole exit plane. In order to minimize the size of the computational grid and the associated computational resource requirements, Choi only modeled a section of the blade that, in the span-wise direction, covered one-half of a film hole pitch with spanwise periodic boundary conditions. Such a reduction in computational span is possible, however, for a linear cascade only, and was also used by Garg and Gaugler (1993, 1994, 1996, 1997a, 1997b). For a rotating blade, the entire span must be discretized in order to model correctly the rotational body forces. Choi obtained a good comparison between the prediction of the surface heat flux with film cooling and the measured data on a 2-D cascade.

The goal of the present study is to provide a comparison between prediction and experiment for the heat transfer coefficient on a film-cooled transonic turbine rotor, including the influence of rotation and three dimensionality. The present approach is to model numerically the exact experimental conditions of an extensive measurement study of Abhari (1991) using the ACE turbine blade. The experimental results without film cooling were used to validate the predictive capability of the 3-D Navier–Stokes code further. Then a number of operating conditions with film cooling were simulated, and the predicted results were compared to the experimental data.

Analysis

The 3-D Navier–Stokes code of Arnone (1994) for the analysis of turbomachinery flows was modified by Garg and Gaugler (1994) to include film cooling effects. Briefly, the code is an explicit, multigrid, cell-centered, finite volume code with an algebraic turbulence model. The Navier–Stokes equations in a rotating Cartesian coordinate system are mapped onto a general body-fitted (ξ, η, ζ) coordinate system using standard techniques. The governing equations, dropping all viscous derivatives in the ξ-direction following the thin-layer approximation (see Garg and Gaugler 1994 for justification), are:

$$\partial_t q + \mathrm{J}[\partial_\xi E + \partial_\eta F + \partial_\zeta G - \mathrm{Re}^{-1}(\partial_\eta F_V + \partial_\zeta G_V)] = H \qquad (1)$$

Notation

B_p	blowing parameter $\{=(\rho_c V_c)/[\rho_o(\mathrm{RT}_o)^{1/2}]\}$
c	sonic speed
c_a	axial chord of the blade
C_D	discharge coefficient for the hole
C_p, C_v	specific heat at constant pressure, and at constant volume, respectively
d	coolant hole diameter
e	total energy
J	Jacobian of the coordinate transformation
k	thermal conductivity
Nu	Nusselt number based on c_a, $(T_{o,\mathrm{rel}} - T_w)$ and k_w
p	pressure
Pr	Prandtl number
Q	total velocity
r	radial coordinate
R	gas constant
R^-	Riemann invariant
Re	Reynolds number based on ρ_o, μ_o sonic speed at T_o and the blade axial chord
s	distance from the leading edge along the pressure or suction surface
S	$= s/s_m$ on suction surface, and $= -s/s_m$ on pressure surface
T	temperature
u, v, w	absolute velocity components in the Cartesian coordinate system
U, V, W	contravariant velocity components
V_c	average coolant velocity at the hole exit
(x, y, z)	Cartesian coordinate system with origin at the geometric stagnation point, and z-coordinate along the span
y^+	dimensionless distance of the first point off the blade surface
z^+	dimensionless distance of the first point off the hub or off the shroud

Greek

β_1	relative flow angle at entry to the rotor
γ	ratio of specific heats
μ	viscosity
ρ	density
Ω	rotational speed of the blade
(ξ, η, ζ)	curvilinear coordinate system with ξ along the wrap-around direction for the C-grid, η running blade-to-blade, and ζ running spanwise

Subscripts

c	for coolant (average value)
e	free-stream (external) value
ef	effective value
ex	value at exit of rotor
ℓ	laminar
m	maximum value
o	stagnation value
rel	value relative to the rotor
t	turbulent
w	at the blade surface

Superscripts

$'$	relative velocity

where

$$q=\begin{bmatrix}\rho\\ \rho U\\ \rho V\\ \rho W\\ e\end{bmatrix}, E=J^{-1}\begin{bmatrix}\rho U'\\ \rho uU'+\xi_x p\\ \rho vU'+\xi_y p\\ \rho wU'+\xi_z p\\ eU'+pU\end{bmatrix},$$

$$F=\mathrm{J}^{-1}\begin{bmatrix}\rho V'\\ \rho uV'+\eta_x p\\ \rho vV'+\eta_y p\\ \rho wV'+\eta_z p\\ eV'+pV\end{bmatrix}, G=\mathrm{J}^{-1}\begin{bmatrix}\rho W'\\ \rho uW'+\zeta_x p\\ \rho vW'+\zeta_y p\\ \rho wW'+\zeta_z p\\ eW'+pW\end{bmatrix}, \tag{2}$$

$$F_v=J^{-1}\mu[0 \quad F_2 \quad F_3 \quad F_4 \quad F_5]^T,$$

$$G_v=\mathrm{J}^{-1}\mu[0 \quad G_2 \quad G_3 \quad G_4 \quad G_5]^T$$

$$H=\Omega[0 \quad 0 \quad -\rho w \quad \rho v \quad 0]^T$$

with

$$F_2=C_1\partial_\eta u+C_2\eta_x+C_3\partial_\zeta u-C_4\eta_x+C_5\zeta_x,$$

$$F_3=C_1\partial_\eta v+C_2\eta_y+C_3\partial_\zeta v-C_4\eta_y+C_5\zeta_y,$$

$$F_4=C_1\partial_\eta w+C_2\eta_z+C_3\partial_\zeta w-C_4\eta_z+C_5\zeta_z,$$

$$F_5=\frac{\mu\gamma}{\mathrm{Pr}}[C_1\partial_\eta(C_vT)+C_3\partial_\zeta(C_vT)]+uF_2+vF_3+wF_4, \tag{3}$$

and

$$C_1=\eta_x^2+\eta_y^2+\eta_z^2, \qquad C_2=\frac{1}{3}(\eta_x\partial_\eta u+\eta_y\partial_\eta v+\eta_z\partial_\eta w),$$

$$C_3=\eta_x\zeta_x+\eta_y\zeta_y+\eta_z\zeta_z, \qquad C_4=\frac{2}{3}(\zeta_x\partial_\zeta u+\zeta_y\partial_\zeta v+\zeta_z\partial_\zeta w),$$

$$C_5=\eta_x\partial_\zeta u+\eta_y\partial_\zeta v+\eta_z\partial_\zeta w \tag{4}$$

Terms multiplied by C_1 and C_2 lead to nonmixed second-derivative viscous terms such as $u_{\zeta\zeta}$, while terms multiplied by C_3, C_4, and C_5 lead to mixed derivative terms such as $u_{\eta\zeta}$. Terms for the viscous flux vector G_v can be written similarly by interchanging η and ζ, and replacing F by G everywhere in Equations 3 and 4.

Solution is obtained in terms of the *absolute* velocity components (u,v,w) in the Cartesian coordinate system (x,y,z) attached to the moving blade, while (U,V,W) are the contravariant and (U',V',W') are the relative contravariant velocity components defined as

$$U=\xi_x u+\xi_y v+\xi_z w, \qquad V=\eta_x u+\eta_y v+\eta_z w,$$

$$W=\zeta_x u+\zeta_y v+\zeta_z w,$$

$$U'=\xi_x u'+\xi_y v'+\xi_z w', \qquad V'=\eta_x u'+\eta_y v'+\eta_z w',$$

$$W'=\zeta_x u'+\zeta_y v'+\zeta_z w' \tag{5}$$

where

$$u'=u, \qquad v'=v-\Omega z, \qquad w'=w+\Omega y \tag{6}$$

are the relative velocity components in the Cartesian system, and Ω is the rotational speed. The energy and static pressure are given by

$$e=\rho\left[C_vT+\frac{1}{2}(u^2+v^2+w^2)\right],$$

$$p=(\gamma-1)\left[e-\frac{1}{2}\rho(u^2+v^2+w^2)\right] \tag{7}$$

Metric terms are defined by

$$\begin{bmatrix}\xi_x & \eta_x & \zeta_x\\ \xi_y & \eta_y & \zeta_y\\ \xi_z & \eta_z & \zeta_z\end{bmatrix}=J\begin{bmatrix}y_\eta z_\zeta-y_\zeta z_\eta & y_\zeta z_\xi-y_\xi z_\zeta & y_\xi z_\eta-y_\eta z_\xi\\ x_\zeta z_\eta-x_\eta z_\zeta & x_\xi z_\zeta-x_\zeta z_\xi & x_\eta z_\xi-x_\xi z_\eta\\ x_\eta y_\zeta-x_\zeta y_\eta & x_\zeta y_\xi-x_\xi y_\zeta & x_\xi y_\eta-x_\eta y_\xi\end{bmatrix} \tag{8}$$

where the Jacobian is given by

$$\mathrm{J}=(x_\xi y_\eta z_\zeta+x_\zeta y_\xi z_\eta+x_\eta y_\zeta z_\xi-x_\xi y_\zeta z_\eta-x_\eta y_\xi z_\zeta-x_\zeta y_\eta z_\xi)^{-1} \tag{9}$$

The equations are nondimensionalized by the inlet total density ρ_o, the blade axial chord as the characteristic length, and $(RT_o)^{1/2}$ as the characteristic velocity. It is assumed that the effective viscosity for turbulent flows can be written as

$$\mu_{\mathrm{ef}}=\mu_\ell+\mu_t \tag{10}$$

where the laminar viscosity μ_ℓ is calculated using Sutherland's law (Schlichting 1979). The turbulent viscosity μ_t is computed using the algebraic mixing length turbulence model of Baldwin and Lomax (1978). This model was designed for the prediction of wall-bounded turbulent shear layers, and may not be appropriate for flows with massive separations or large vortical structures. Thus, this model is likely to be invalid in a number of turbomachinery applications, but for turbine blades, the boundary layers generally experience a favorable pressure gradient whereby this model is more likely to be valid. It has been used satisfactorily by Boyle and Giel (1992). Ameri and Arnone (1994, 1996), and Boyle and Ameri (1997) for heat transfer calculations on turbine blades without film cooling, and by Hall et al. (1994) and Garg and Gaugler (1994) with film cooling. In fact, Ameri and Arnone (1994) compared the Baldwin–Lomax model and Coakley's q-ω model (Coakley 1983) against experimental data of Graziani et al. (1980), and found that the algebraic model was able to produce many of the flow features better than the two-equation model. They further state that this conclusion is strengthened when we take into account the relative economy of computations with the algebraic model. It is known (Amer et al. 1992) that two-equation models are also not satisfactory in the presence of film cooling. Perhaps the multiple time-scale turbulence model of Kim and Benson (1992) may be more appropriate. However, use of this model is computationally very expensive, because it involves solving four more partial differential equations in addition to the five at present, all coupled.

Boundary conditions

At the inflow boundary, the total temperature, total pressure, whirl, and meridional flow angle are specified, and the upstream-running Riemann invariant R^- based on the total absolute velocity is calculated at the first interior point and extrapolated to the inlet. The Riemann invariant is given by

$$R^- = Q - 2c/(\gamma - 1) \tag{11}$$

The total velocity is found from T_o and R^- using

$$Q = \frac{(\gamma - 1)R^- + \sqrt{2(1-\gamma)(R^-)^2 + 4(\gamma+1)C_pT_o}}{\gamma + 1} \tag{12}$$

The velocity components are then decoupled algebraically, and the density is found from p_o, T_o, and Q using an isentropic relation.

At the exit, the hub static pressure is specified, and the density and velocity components are extrapolated from the interior. The local static pressure is found by integrating the axisymmetric radial equilibrium equation. Periodic flow conditions in terms of cylindrical velocity components are set on a dummy grid line outside the boundary. On the blade surface and the rotating part of the hub, $U' = V' = W' = 0$. The experimental values for the blade temperature were known at only 25 points on the blade surface, while the computational grid had over 38,000 grid points on the blade surface. Thus, in the absence of a complete surface temperature map, the blade surface was considered isothermal. The largest experimental variations in the blade surface temperature relative to the mean were as much as 10% from the mean for the fully film-cooled test cases. The hub and shroud surfaces were also considered isothermal and assumed to be at the same temperature as the blade. Based upon an estimate obtained from a streamline curvature prediction, the boundary-layer thickness on the hub and shroud was taken to be 10 and 15% of span for the incoming flow to the rotor.

The effects of film cooling have been incorporated into the code in the form of appropriate boundary conditions at the hole locations on the blade surface. The vena contracta of each hole was accounted for by reducing the actual hole exit area by the values of the estimated discharge coefficients C_D reported in Table 1. Each hole exit is represented by several control volumes having a total area equal to the area of the hole exit, and passing the same coolant mass flow, with the discharge coefficient for the hole having been taken into account. Different velocity and temperature profiles for the injected gas can be specified at the hole exit. For the cases reported here, uniform profiles for the coolant velocity (relative to the blade) and temperature distribution at the hole exit were specified. Also, one case was run with a polynomial distribution (Garg and Gaugler 1997b) of coolant velocity and temperature at the exit of the double-row of holes on the pressure surface in order to ascertain if that would bring the predicted and experimental results closer on the pressure surface.

The four-stage Runge–Kutta scheme developed by Jameson et al. (1981) is used to advance the flow solution in time from an initial guess to the steady state. To accelerate convergence, the code employs the full approximation storage (FAS) multigrid method originally devised by Brandt (1979) and Jameson (1983). Variable coefficient implicit smoothing of the residuals is performed to improve further the rate of convergence. A (3-D) extension of eigenvalue scaling of the artificial dissipation terms, first devised by Martinelli (1987), was adopted to prevent odd–even decoupling and to capture shocks. Further details of the numerical scheme and implementation of the boundary conditions are given in Arnone (1994).

Table 1 Parameter values

Main flow parameters: $R = 125.1$ J/kg-K

Case	p_o (kPa)	T_o (K)	p_{ex} (kPa)	Ω (rpm)	T_w (K)	γ
71	450.0	486.0	117.537	7087	321.3	1.246
72	460.0	490.0	128.683	5610	325.0	1.255
73	351.0	417.0	92.206	6330	310.0	1.276
61	458.0	500.0	93.219	7380	310.0	1.237

Coolant flow parameters: $R_c = 158.5$ J/kg-K

Case	γ_c	$T_{o,rel}$ (K)	$p_{o,rel}$ (kPa)		
			Hub	Midspan	Tip
71	1.406	222.5	241.761	255.238	262.229
72	1.405	224.5	258.683	268.410	275.503
73	1.406	222.9	194.645	204.373	212.276

Hole characteristics: Hole diameter = 0.5 mm, spanwise pitch = 2 mm, spanwise angle = 90°

Hole-row	Estimated discharge coefficient C_D									Streamwise angle (deg)	Hole Shape	No. holes
	Hub for case			Midspan for case			Tip for case					
	71	72	73	71	72	73	71	72	73			
PS1	0.52	0.63	0.57	0.64	0.66	0.64	0.63	0.67	0.66	60	Cylinder	18
PS21	0.50	0.63	0.62	0.62	0.64	0.64	0.60	0.65	0.65	30	Cylinder	19
PS22	0.56	0.63	0.61	0.62	0.64	0.63	0.64	0.65	0.64	30	Cylinder	18
SS1	0.52	0.37	0.52	0.59	0.45	0.56	0.62	0.56	0.61	30	D-shape	18
SS2	0.48	0.48	0.48	0.39	0.39	0.39	0.46	0.46	0.46	30	Cylinder	20

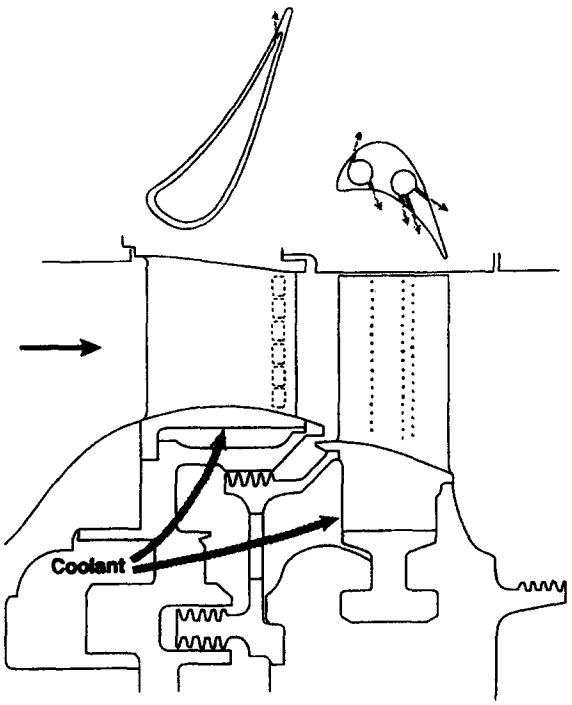

Figure 1 ACE turbine geometry and cooling arrangement

ACE Rotor and experimental details

The Rolls-Royce ACE high-pressure transonic turbine model was the test object on which film cooling data were taken in the short duration (0.3 s measurement time), blowdown, rotating turbine rig facility at MIT by Abhari (1991). In this facility, it is possible to simulate full engine-scale Reynolds number, Mach number, Prandtl number, gas-to-wall and coolant-to-mainstream temperature ratios, specific heat ratios, and flow geometry while operating under benign conditions. The turbulent intensity at the nozzle guide vane inlet was less than 1%. A mixture of argon and freon-12 was used for the main flow, and a mixture of argon and freon-14 was used as the coolant to prevent condensation at the low temperatures and high pressures of the coolant supply system. Values of the gas constant and specific heat ratios for the mainstream and coolant flows are given in Table 1.

The ACE turbine geometry and cooling arrangement are shown schematically in Figure 1. This turbine had a 551.2-mm rotor diameter with 36 nozzle guide vanes (NGVs) and 61 rotor blades. The rotor blades had an axial chord of 26.1 mm, and five film-cooling rows containing 93 holes. For the cooled rotor tests, thin-walled NGVs were used with slot injection near the pressure surface trailing edge, sized to pass the flow of a fully cooled NGV. Three instrumented and six other solid aluminum rotor blades were drilled out for two radially positioned coolant supply plenums; the other 52 rotor blades were of steel shell construction. The coolant film hole internal diameter was 0.5 mm for all holes. All rows had circular exit areas except for the first row (SS1) on the suction surface, which was D-shaped. The cooling configuration consisted of: (1) one 30° single row (SS1) of 18 D-shaped holes (fanned at 25° half angle in the spanwise direction with an exit width of 1.25 mm) at about 20% surface length on the suction surface; (2) one 30° single row (SS2) of 20 round holes at about 70% surface length on the suction surface; (3) one 60° single row (PS1) of 18 holes at about 25% surface length on the pressure surface; and (4) one 30° double row of 19 (PS21) and 18 (PS22) staggered holes, with a chordwise spacing of 2 mm, at about 50% surface length on the pressure surface. All holes were drilled at 90° from the radial direction. More details in terms of estimated discharge coefficient for the holes are available in Table 1. Figure 2 shows a small portion of the unfolded part of the blade containing the holes. The ordinate in Figure 2 denotes the distance along the blade surface in the spanwise direction, while the abscissa denotes the distance, measured from the leading edge, along the blade surface in the streamwise direction, both normalized by the hole diameter d. The shape and orientation of the hole openings in Figure 2 is a direct consequence of the angles the holes make with the spanwise or streamwise direction.

The heat flux from the free stream to the blade was measured with thin-film heat flux gauges distributed about the blade profile. These transducers are 25-μm thick with a rectangular sensing area (1.0 × 1.3 mm), oriented so that the longest dimension is in the chordwise direction. The coolant hole and heat flux gauge locations are shown in Figure 3. The top chordwise row is referred to as the tip location, the middle as midspan, and the bottom as the hub gauges. Note that none of the three rows of gauges is at a fixed radial location. Unfortunately, several of the gauges failed over the course of the testing, especially on the pressure surface. Thus, not all measurement locations yielded data at all test conditions. High-frequency response pressure transducers and thermocouples were installed in the NGVs and rotor blades to monitor the conditions in the coolant hole supply plenums. All worked well except for the rotor thermocouples, which were unreliable. Facility measurements included inlet total temperature and pressure, outlet total pressure, wall static pressures, and rotor speed. More details are available in Abhari (1991).

Computational details

The grid size is nonuniform in all directions so as to pack more grid points within the hole exits and near the boundary layers on the blade, the hub, and the shroud. For computational accuracy, the ratio of two adjacent grid sizes in any direction was kept within 0.76–1.3. A periodic C-grid with over 2,278,000 grid points was used. The grid used was 225 × 45 × 225, where the first number represents the number of grid points along the wrap-around direction for the C-grid, the second in the blade-to-blade direction, and the third in the span direction. This grid was arrived at following numerical experimentation with a coarser grid, 133 × 41 × 113, and discussions with co-workers. Normal to the blade surface is the dense viscous grid, with $y^+ < 1.0$ for the first point off the blade surface, following Boyle and Giel (1992) and Hall et al. (1994). Normal to the hub and shroud also is a dense grid, with $z^+ < 2.5$ for the first point off the hub or off the shroud. Also, the tip clearance region was taken to be 1% of the blade span (static measurement) with 20 grid points within it. The tip clearance region is handled by imposing periodicity conditions across the airfoil. Computations were run on the 16-processor C-90 supercomputer at NASA-Ames Research Center. The code requires about 130 million words (Mw) of storage

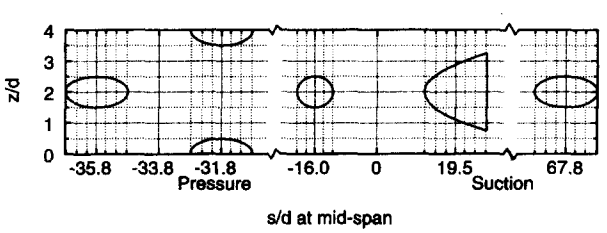

Figure 2 Shape of film-cooling holes at exit on the ACE rotor surface

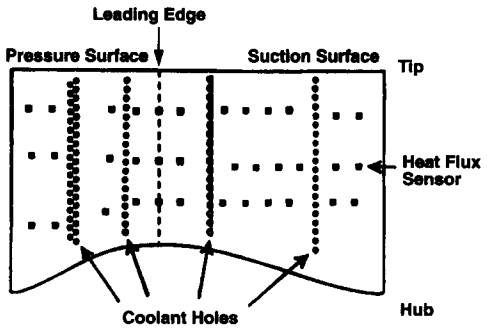

Figure 3 Heat flux gauges and cooling hole locations on the projected blade surface with each of the three chordwise rows of gauges on a separate blade

and takes about 45 s per iteration (full multigrid) on the C-90 machine. For a given grid, the first isothermal blade case requires about 1000 iterations to converge, while subsequent cases (corresponding to different values of the parameters) for the same grid require about 400 iterations, starting with the solution for the previous case.

Results and discussion

The present numerical results were obtained by simulating the exact experimental conditions of the MIT experiment given in Table 1 for the cases compared. The blowing parameter B_p and the coolant temperature T_c/T_o at the hole exits were estimated from the static pressure distribution on an uncooled blade (found by executing the present code in the uncooled mode), and the relative total pressure and temperature measured in the coolant plenums, with coolant Mach number, relative to the rotor, restricted to unity at the hole exit. All holes in the second row (SS2) and most holes in the first row (SS1), especially those near the hub, on the suction surface were choked. In addition to the three film-cooled cases, Runs 71, 72, and 73, an uncooled case, Run 61, was also selected for comparison, as detailed in Table 1. While case 71 represents near design-condition operation, test case 73 represents a lower pressure ratio and speed, and case 72 has a positive incidence angle. Figure 4 shows the computed relative flow angle at the rotor inlet; the symbols in this figure represent the predicted values from a through-flow streamline curvature calculation, while the curves belong to the 3-D calculation based on the present code. The effect of boundary layers on the hub and shroud is clearly reflected in Figure 4.

Figure 5 compares the computed Nusselt number on the blade surface near the midspan with the experimental data for the nonfilm cooled case 61. The Nusselt number is based on the rotor axial chord, the relative total temperature at entry to the rotor, the blade temperature, and the gas thermal conductivity at the blade temperature. The abscissa is the fractional wetted pressure and suction surface of the blade. The experimental data are shown with error bars. Comparison at the leading edge and all along the suction surface is very good (within 10%), but on the pressure surface, the prediction is approximately 30% lower than the data at all locations. This comparison suggests that, in the absence of film cooling, the present approach is correctly simulating the driving mechanisms for heat transfer on the suction surface. Reasons for the underprediction on the pressure surface are cited later.

Figure 6 compares the computed Nusselt number on the blade surface near the hub, midspan, and tip with the experimental data for the film-cooled baseline case 71. Presence of negative values of Nu at some locations simply implies that the

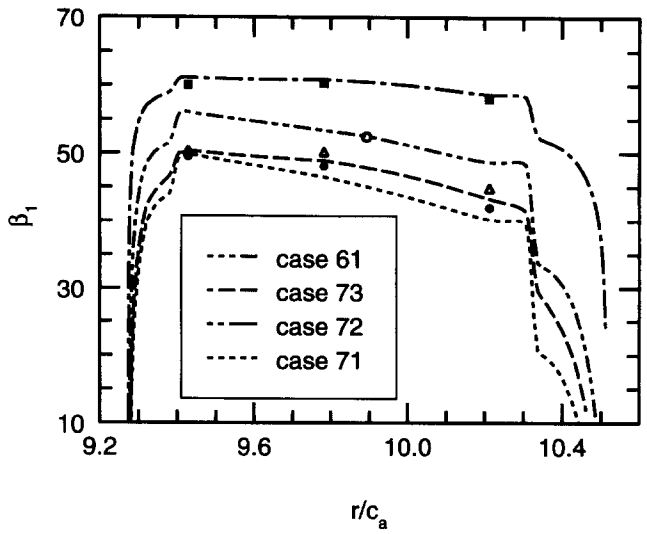

Figure 4 Relative flow angle at rotor inlet as a function of spanwise location

direction of heat transfer is reversed at these locations because of specification of the isothermal wall boundary condition and coolant temperature. The comparison is very good at the leading edge, generally good on the suction surface, but fairly poor downstream of PS1 on the pressure surface near the hub. It is interesting to note that near the hub section, where the best experimental data coverage is available, the suction surface heat transfer is very well predicted, both in terms of the level and the distribution of surface heat flux. On the pressure surface, however, the prediction completely underpredicts the heat transfer.

In Figures 7 and 8, similar comparisons of numerical prediction of Nusselt number with the experimental data for film-cooled cases 72 and 73 are shown, respectively. There are a number of possible reasons for the poor comparison with the experimental data on the pressure surface. There is a strong evidence (Abhari 1996) that the periodic flow unsteadiness resulting from the stator–rotor interaction fundamentally changes the coolant jet/main flow interaction on the pressure surface, while the suction surface is relatively unaffected. The present calculation, being steady state, does not model this unsteadiness. In the experimental tests, however, the rotor blades interact with the shock,

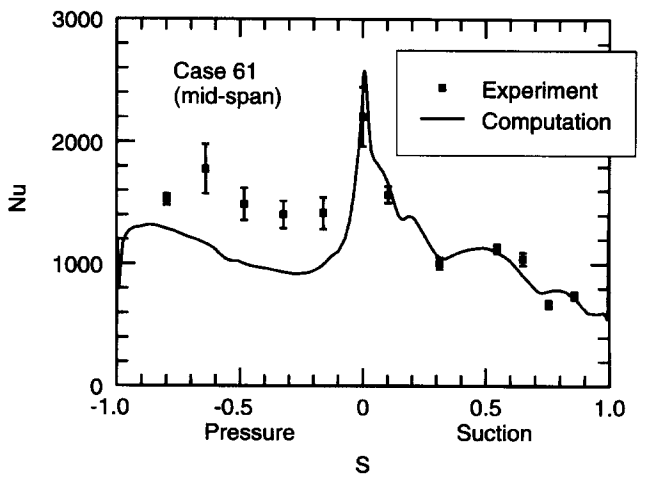

Figure 5 Comparison of Nusselt number on the blade surface for uncooled case 61 near midspan

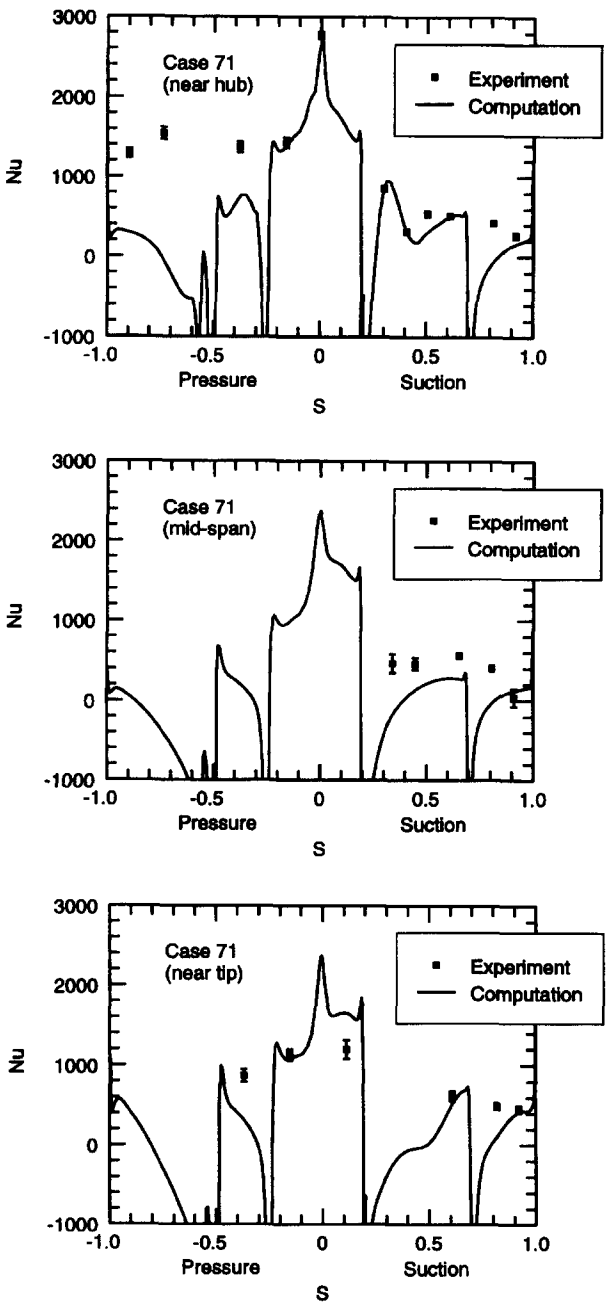

Figure 6 Comparison of Nusselt number on the blade surface for case 71 near hub, midspan, and tip

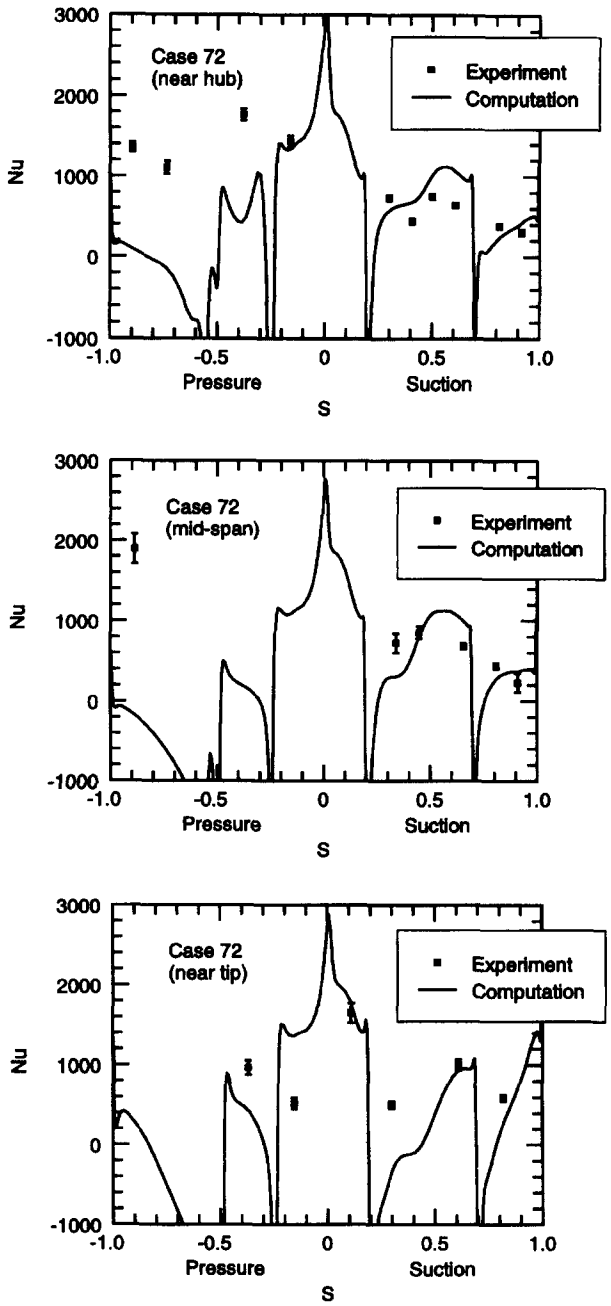

Figure 7 Comparison of Nusselt number on the blade surface for case 72 near hub, midspan, and tip

wakes, and the potential field of the upstream nozzle guide vanes, resulting in a highly unsteady flow structure (Abhari et al. 1992). This is true whether the blade is cooled or uncooled. Another possible cause of this discrepancy for the cooled rotor can be the result of uncertainty in the values of the blowing parameter, coolant temperature, and the relative flow angle at inlet to the rotor, which were all estimated by matching the values from a through-flow streamline curvature calculation, in the absence of experimental measurements, with the present code. Also, the gas constant and specific heat ratios for the mainstream and coolant flow are different in the experiment because of the use of different gas mixtures, but the code assumes the same gas for both the main and coolant flows. Moreover, values of the discharge coefficients for the film-cooling holes were estimated, not measured. Additionally, the spanwise diffusivity is much higher than that in the direction normal to the blade. Finally, it is possible that the turbulent mixing on the low-Mach number pressure surface is underpredicted by the turbulence model. Although the results in Figures 6–8 are based on a uniform coolant velocity and temperature distribution at the hole exits, specifying a polynomial distribution, such as that in Garg and Gaugler (1997b), at the exit of the double row of holes on the pressure surface does not improve the comparison by more than 5%.

In Figure 9, the present 3-D computation of Nusselt number is compared with the predictions from a 2-D Navier–Stokes code with a film injection model (Abhari 1996) and experimental data for cases 71 and 72 near midspan. The 2-D calculation seems to

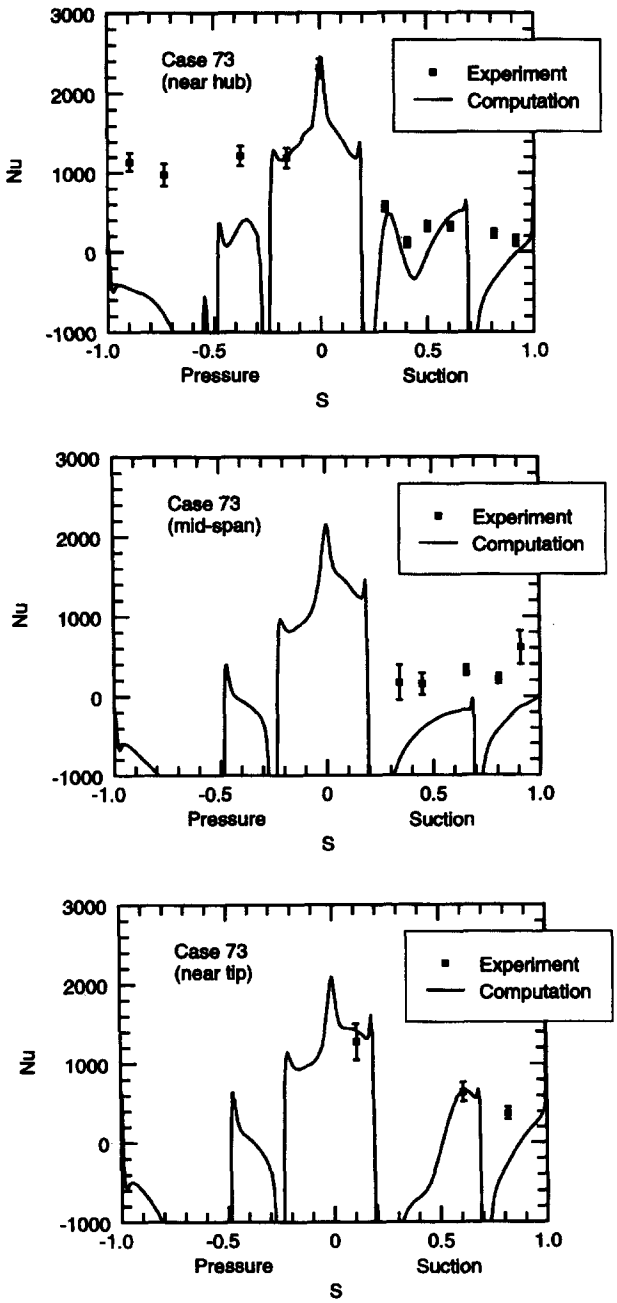

Figure 8 Comparison of Nusselt number on the blade surface for case 73 near hub, midspan, and tip

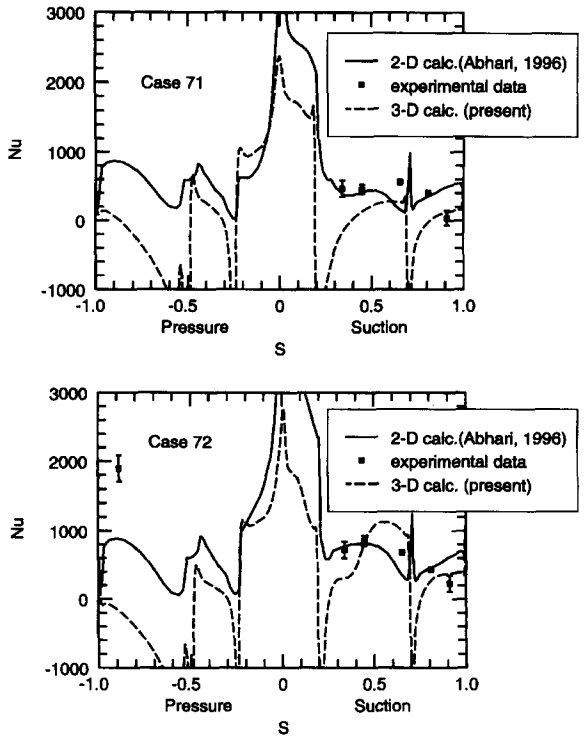

Figure 9 Comparison of Nusselt number on the blade surface for cases 71 and 72 near midspan

give a higher level of the Nusselt number values compared to the 3-D code almost everywhere around the airfoil. The predictions from the present 3-D code provide a much better comparison to the experimental data for the leading edge heat transfer than the 2-D prediction reported by Abhari (1996). Figure 10 shows Nusselt number contours at increments of 200 over the entire blade surface for the one uncooled and three cooled cases. Because there is no film cooling over the leading-edge portion, this part of the blade has a high Nusselt number, being exposed to the hot stream for all the four cases. Downstream of the first and subsequent rows of cooling holes on both the pressure and suction surfaces, the effect of film cooling is clearly evident as streaks of lower heat load and generally lower Nusselt number values as compared to the uncooled case. For the off-design case 72, the blade suction surface upstream of the second row of holes has higher Nusselt number values than the other cooled cases. It also has higher Nu values on the leading-edge portion. On the other hand, case 73 has lower Nu values than all the other cases over the entire blade surface, and is, thus, the best-cooled case studied. It may also be observed that the Nusselt number is fairly

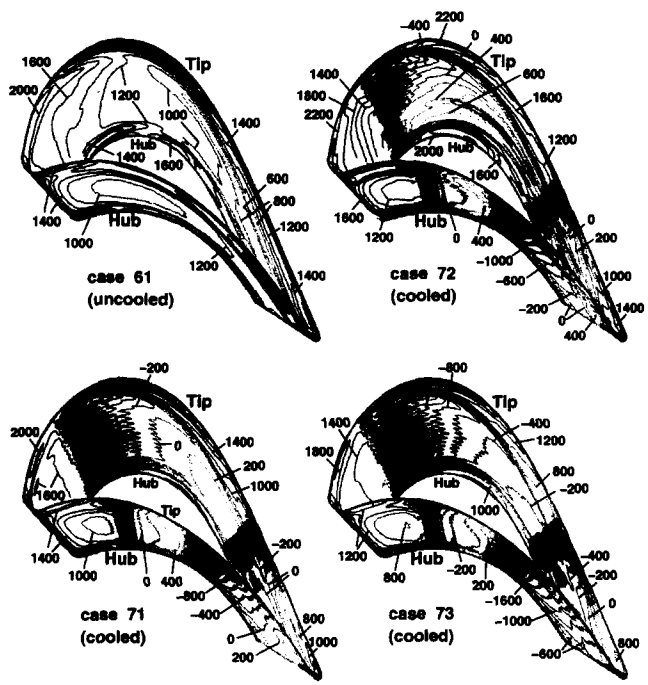

Figure 10 Nusselt number contours on the ACE rotor for various cases

high in the thick boundary layers on the suction surface near both the hub and the tip. From this figure, we observe that the Nusselt number is a strong function of the streamwise as well as the spanwise location, especially in the vicinity of film-cooling holes.

Conclusions

As far as the authors know, the present study provides the first comparison of surface heat transfer between a fully 3-D Navier–Stokes code with film injection and the experimental data obtained on a transonic rotating rotor blade with film cooling. The present approach was shown to provide a reasonably good prediction of the heat transfer at the leading edge and on the suction surface of a film-cooled rotor blade when compared to the experimental data, validating the code under blade rotation. On the pressure surface, the code underpredicted the surface heat transfer. Reasons for differences on the pressure surface are cited; the most plausible one seems to be the presence of unsteady effects because of stator–rotor interaction in the experiments, which are neglected in the present computations. It is found that the Nusselt number on the blade surface is highly 3-D in the vicinity of holes but tends to become 2-D far downstream.

Acknowledgments

The first author thanks Raymond Gaugler, Chief, Turbine Branch, and John Rohde of the Subsonic Systems Office at the NASA-Lewis Research Center for their support of this work. The experimental results reported in this work were supported by the Wright Laboratories, USAF, C. McArthur, program monitor, and Rolls-Royce Inc., R. J. G. Norton, technical monitor. A part of this work was presented as ASME paper 96-GT-223; we acknowledge permission from ASME to publish it.

References

Abhari, R. S. 1991. An experimental study of the unsteady heat transfer process in a film-cooled fully scaled transonic turbine stage. Ph.D. thesis, Massachusetts Institute of Technology, Cambridge, Massachusetts, USA

Abhari, R. S. 1996. Impact of rotor–stator interaction on turbine blade film cooling. *J. Turbomachinery*, **118,** 123–133

Abhari, R. S. and Epstein, A. H. 1994. An experimental study of film cooling in a rotating transonic turbine. *J. Turbomachinery*, **116,** 63–70

Abhari, R. S., Guenette, G. R., Epstein, A. H. and Giles, M. B. 1992. Comparison of time-resolved measurements and numerical calculations. *J. Turbomachinery*, **114,** 818–827

Amer, A. A., Jubran, B. A. and Hamdan, M. A. 1992. Comparison of different two-equation turbulence models for prediction of film cooling from two rows of holes. *Numer. Heat Transfer*, **21A,** 143–162

Ameri, A. A. and Arnone, A. 1994. Prediction of turbine blade passage heat transfer using a zero and a two-equation turbulence model. ASME paper 94-GT-122

Ameri, A. A. and Arnone, A. 1996. Transition modeling effects on turbine rotor blade heat transfer predictions. *J. Turbomachinery*, **118,** 307–313

Arnone, A. 1994. Viscous analysis of three-dimensional rotor flow using a multigrid method. *J. Turbomachinery*, **116,** 435–445

Baldwin, B. S. and Lomax, H. 1978. Thin-layer approximation and algebraic model for separated turbulent flows. AIAA paper 78-257

Boyle, R. J. and Ameri, A. A. 1997. Grid orthogonality effects on predicted turbine midspan heat transfer and performance. *J. Turbomachinery*, **119,** 31–38

Boyle, R. J. and Giel, P. 1992. Three-dimensional Navier–Stokes heat transfer predictions for turbine blade rows. AIAA paper 92-3068

Brandt, A. 1979. Multilevel adaptive computations in fluid dynamics. AIAA paper 79–1455

Choi, D. 1993. A Navier–Stokes analysis of film cooling in a turbine blade. AIAA paper 93-0158

Coakley, T. J. 1983. Turbulence modeling methods for the compressible Navier–Stokes equations. AIAA paper 83-1693

Crawford, M. E., Kays, W. M. and Moffat, R. J. 1980. Full coverage film cooling on flat, isothermal surfaces: A summary report on data and predictions. NASA CR 3219

Dring, R. P., Blair, M. F. and Joslyn, H. D. 1980. An experimental investigation of film cooling on a turbine rotor blade. *J. Eng. Power*, **102,** 81–87

Garg, V. K. and Gaugler, R. E. 1993. Heat transfer in film-cooled turbine blades. ASME paper 93-GT-81

Garg, V. K., and Gaugler, R. E. 1994. Prediction of film cooling on gas turbine airfoils. ASME paper 94-GT-16

Garg, V. K. and Gaugler, R. E. 1996. Leading-edge film-cooling effects on turbine blade heat transfer. *Numer. Heat Transfer*, **30A,** 165–187

Garg, V. K. and Gaugler, R. E. 1997a. Effect of coolant temperature and mass flow on film cooling of turbine blades. *Int. J. Heat Mass Transfer*, **40,** 435–445

Garg, V. K. and Gaugler, R. E. 1997b. Effect of velocity and temperature distribution at the hole exit on film cooling of turbine blades. *J. Turbomachinery*, **119,** 343–351

Goldstein, R. J. 1971. Film cooling. *Adv. Heat Transfer*, **7,** 321–379.

Graziani, R. A., Blair, M. F., Taylor, J. R. and Mayle, R. E. 1980. An experimental study of endwall and airfoil surface heat transfer in a large-scale turbine blade cascade. *J. Eng. Power*, **102,** 257–267

Hall, E. J., Topp, D. A., and Delaney, R. A. 1994. Aerodynamic/heat transfer analysis of discrete site film-cooled turbine airfoils. AIAA paper 94-3070

Jameson, A. 1983. Transonic flow calculations. MAE report. 1651, MAE Department, Princeton University, Princeton, NJ

Jameson, A., Schmidt, W. and Turkel, E. 1981. Numerical solutions of the Euler equations by finite-volume methods using Runge–Kutta time-stepping schemes. AIAA paper 81-1259

Kim, S.-W. and Benson, T. J. 1992. Calculation of a circular jet in cross flow with a multiple-time-scale turbulence model. *Int. J. Heat Mass Transfer*, **35,** 2357–2365

Martinelli, L. 1987. Calculations of viscous flows with a multigrid method. Ph.D. thesis, Princeton University, Princeton, NJ

Schlichting, H. 1979. *Boundary Layer Theory*, 7th ed., McGraw-Hill, New York, 328

Schönung, B. and Rodi, W. 1987. Prediction of film cooling by a row of holes with a two-dimensional boundary-layer procedure. *J. Turbomachinery*, **109,** 579–587

Tafti, D. K. and Yavuzkurt, S. 1990. Prediction of heat transfer characteristics for discrete hole film cooling for turbine blade applications. *J. Turbomachinery*, **112,** 504–511

Takeishi, K., Aoki, S., Sato, T. and Tsukagoshi, K. 1991. Film cooling on a gas turbine rotor blade. ASME paper 91-GT-291